ST-ECF Instrument Science Report WFC3-2009-01

The ground calibrations of the WFC3/UVIS G280 grism

H. Kuntschner, H. Bushouse, M. Kümmel, J. R. Walsh
January 15, 2009

ABSTRACT

Based on thermal vacuum tests (TV2; June - August 2007and TV3; March/April 2008), the performance of the WFC3 UV G280 grism has been assessed. The locations of the different orders relative to exposures taken through a direct imaging filter are determined, trace and wavelength solutions are derived for a central position on each chip, and the absolute throughput of the different orders is quantified. Aperture corrections are given as a function of wavelength. Furthermore, we describe flat-field cubes that provide pixel-to-pixel information as a function of wavelength to an accuracy of about 2%.
The $+1^{st}$ order is useful for scientific observations in the range ~190 to 500nm, however, the $+2^{nd}$ order spectrum is overlapping with the first order for wavelengths larger than about 390nm. For wavelengths above ~320nm, the 0^{th} order, which shows a small dispersion, carries more power than the $+1^{st}$ order. Therefore, especially for red sources, the 0^{th} order is prone to saturation effects. The trace and wavelength solutions show significant variations as a function of position within the field-of-view. However, the available ground calibrations are not sufficient to establish a full position-dependent calibration. Henceforth, the calibrations reported in this ISR can only be used to extract spectra of relatively isolated, blue targets placed at the central position on Chips 1 or 2.

1. Introduction

The Wide Field Camera 3 (WFC3) is fitted with three grisms for slitless spectroscopy. In the UVIS channel there is one grism, G280, for the near-UV to visible range (200 - 400nm). The NIR channel has two grisms (G102 and G141) for the shorter (800 - 1150nm) and longer NIR wavelengths (1100-1700nm).

The fundamental design parameters of a grism are the deflection of the incident beam by the grism (defined by the prism angle), dispersion in the various orders and the energy in each order (defined by the groove frequency and profile). In order to extract slitless spectra from grism images it is necessary to know these parameters and their variation with position in the field. With a good parameterization, then extraction software, such as the aXe task developed at the ST-ECF (http://www.stecf.org/software/slitless_software), can be applied to extract multiple slitless spectra from sky images in a semi-automatic fashion. A further use of the parameterization is to provide a simulation package that can predict two-dimensional dispersed images of a given sky region if an input catalogue is provided. The ST-ECF has developed such a package for Cycle 17 (aXeSIM; Kümmel, Kuntschner, Walsh 2007; Kümmel et al. 2009).

During the Thermal Vacuum testing of WFC3 in June - August 2007 (TV2) and March/April 2008 (TV3), specific calibrations for the UVIS grism were included. The tests were designed to allow determination of the spectral trace, the dispersion solution and the absolute instrument throughput by using a combination of monochromator and white light source measurements. Additionally, the detector flat-field was determined with narrowband exposures. This ISR describes the implementation of the tests and the analysis of the results; emphasis is given to the results from TV3 where the flight detectors were installed in WFC3. Tables provide the details of the trace and the dispersion solution; measurements of the total instrument throughput and information on the wavelength dependent flat-field are also provided.

This instrument science report (ISR) is a follow-up on the report by Larsen, Bushouse, & Walsh (WFC3-2005-17) from the TV1 calibrations.

2. Calibration setup in TV2 and TV3

The grism test procedures were executed in TV2 and TV3 with the WFC3 in a flight-like thermal-vacuum environment. The WFC3 external optical stimulus system, CASTLE, was used to provide the necessary source targets for the tests. For these tests, the WFC3 detector UVIS-2 was used in TV2 and UVIS-1 was used in TV3; the detectors were most of the time at an operating temperature of -83°C. For the dispersion and spectral trace calibration procedures we used sets of point-source exposures, all of which were obtained with the CASTLE quartz-tungsten-

halogen (QTH) lamp, and a 10-micron pinhole to provide an unresolved target. An extended source (200 micron pinhole) was used to provide high S/N photometric measurements for the absolute instrument throughput calibrations with the G280 grism in place.

3. Calibration measurements

For the UVIS G280 grism, calibration measurements were carried out to allow determination of the spectral trace, the dispersion solution and the absolute instrument throughput as well as a wavelength dependent flat-field. A high level summary of all UVIS grism calibration procedures in TV2 and TV3 is given in Tables 1 and 2, respectively. During TV2 trace and dispersion calibrations were performed in a 5-point pattern (one central position and the four quadrants) to allow for a 2-dimensional solution covering the field-of-view (FoV) of Chip 1+2. A central position on Chip 1 was calibrated for absolute throughput. In TV3 trace and dispersion calibrations were performed only for one central position on each of the chips (see Table 3). Absolute throughput is determined for one position on each of the chips.

Table 1. Summary of UVIS grism calibrations from TV2

Test procedure	Date	Grism	Purpose
UV21S04	**2007-07-15**	**G280**	**Flat field in Thermal Vac Chip 1+2**
UV21S02A	**2007-07-27**	**G280**	**Absolute throughput Chip 1**
UV21S05	**2007-10-10**	**G280**	**Absolute throughput Chip 1 wavelength extension to the red**
UV24S02A	**2007-07-04**	**G280**	**Dispersion (centre) Chip 1**
UV24S02A	**2007-08-01**	**G280**	**Dispersion (centre) – repeat Chip 1**
UV24S05	**2007-08-01**	**G280**	**Dispersion (quadrant A) Chip 1**
UV24S04	**2007-08-01**	**G280**	**Dispersion (quadrant B) Chip 1**
UV24S06	**2007-08-02**	**G280**	**Dispersion (quadrant C) Chip 2**
UV24S03	**2007-08-01**	**G280**	**Dispersion (quadrant D) Chip 2**

Table 2. Summary of UVIS grism calibrations from TV3

Test procedure	Date	Grism	Purpose
UV21S02B	**2008-03-18**	**G280**	**Absolute throughput Chip 1**
UV21S07	**2008-04-04**	**G280**	**Absolute throughput Chip 2**
UV21S04A	**2008-04-29**	**G280**	**Flat field in Thermal Vac Chip 1+2**
UV21S06	**2008-04-30**	**G280**	**Flat field in ambient Chip 1+2**
UV24S07	**2008-04-05**	**G280**	**Dispersion (centre Chip 1)**
UV24S08	**2008-04-09**	**G280**	**Dispersion (centre Chip 2)**

The absolute throughput measurements were carried out with a calibrated monochromator source covering wavelengths from 190 to 1000nm (note, that only during TV3 the full wavelength range was covered). The trace and dispersion calibrations were carried out starting with a set of direct image and grism pairs using a white light stimulus. After that monochromator steps covering the range 200-530nm in steps of 15nm for TV2 and 200-915nm in TV3 in increasing steps of 15, 25 and 100nm were performed. In all cases, the monochromator bandwidth was 10 nm.

Additionally, the detector flat-field with full frame illumination was determined in TV2 with 13nm wide bandpasses in steps of 30nm, covering the range 260-530nm; in TV3 with 13nm wide bandpasses in steps of 30nm, covering the range 260-530nm with an additional set at 200, 220 and 240nm taken with 16nm wide bandpasses.

4. Analysis

In this section we describe the analysis of the calibration data yielding calibrations for the trace and wavelength solutions and the absolute throughput. The field-dependent trace and dispersion data obtained during TV2 for Chip 1+2 showed that the field dependent solutions are complex and cannot be easily expressed in the aXe parameterisation (i.e. surface polynomial fits), at least not with only 5 different field positions available for the calibration (see also Figure 11). Furthermore, during TV3, with the flight detector inserted, only one (central) standard source position could be calibrated for each chip. Therefore, in this ISR we concentrate on the analysis and description of the calibration for these two standard positions (see Table 3) as determined in TV3.

Table 3: Central standard positions on each chip for the trace and dispersion solutions as derived in this ISR from TV3 data.

	X0	Y0
Chip 1	2135.15	864.02
Chip 2	2151.27	872.25

4.1. Trace calibration

The ST-ECF aXe package for reduction of slitless spectroscopy data treats the spectral traces and wavelength solutions defined with respect to the position of the

source in the direct image (Kümmel et al. 2009). The centroids of the continuum source images in the direct imaging exposures (X_{ref}, Y_{ref}) were determined with the IRAF task imexam. These positions were assumed not to change through the duration of the remaining measurements. For the G280 grism there is a rather large offset of about 170 pixels in the y-direction between the position of the source in the direct image and the $+1^{st}$ order spectrum (see Figure 1). The observation of a continuum lamp spectrum with the G280 grism shows that many orders are visible and largely overlapping with each other (see Figure 1). Due to this heavy overlap, the typical approach of tracing the continuum spectrum as a function of $\Delta X=X-X_{ref}$ in the CCD X-direction is not feasible here. Instead we used the monochromator steps observed for the dispersion calibrations (see also Section 4.2) to obtain accurate trace information. For each wavelength setting the position of the $+3^{rd}$ to -3^{rd} orders as observed in TV3 was determined with the IRAF task imexamine (see also Figure 2). Several points are noteworthy: (a) The 0^{th} order is weakly dispersed, spanning about 23 pixels in the y-direction for wavelengths of 200 to 915nm; (b) the $+1^{st}$ order (defined as the order carrying the maximum throughput in the UV and hence the one extending to decreasing x-axis pixels towards the left of the 0^{th} order) follows a highly curved trace and overlaps with the $+2^{nd}$ order in x-direction for wavelengths larger than about 390nm. The same is true for the -1^{st} and -2^{nd} order spectra; (c) higher orders (negative and positive) strongly overlap in the x-direction and are essentially merging into a single spectrum. Hence the observation of a reasonably bright source placed near the chip centre in the x-direction affects a semi-contiguous band of pixels across the full x-extension of the detector.

In TV3 only one central position was calibrated for each chip (see Table 3). Using the trace information from the monochromator steps we determine trace solutions for the $+3^{rd}$ to -3^{rd} spectral orders for wavelength between 200 and 815nm; the monochromator step at 915nm was omitted in the trace analysis since, for unknown reasons, it did not follow the general trends. Due to S/N limitations there is only reduced information for higher spectral orders available, but not considered in this ISR. The results of the trace fits are given in Tables 4 and 5, respectively.

The trace definitions are of the form $(Y-Y_{ref})=DYDX\_0 + DYDX\_1*\Delta X + DYDX\_2*\Delta X^2 + DYDX\_3*\Delta X^3 + DYDX\_4*\Delta X^4$ where DYDX_0-4 are normally field dependent and given in the usual format used by the ST-ECF aXe reduction package, e.g., $DYDX\_1 = a0 + a1*X_{ref} + a2*Y_{ref} + \ldots$(see also the aXe manual for more details). During TV2 several positions (5-point pattern for each chip) across the field were calibrated. However, attempts to establish a stable, field dependent solution failed due to (a) significant and complex variations of the trace shape across the field-of-view (see also Figure 11); and (b) the lack of enough calibration points to sample the field dependent variations. In conclusion, we can currently provide a calibration for the trace and wavelength solution only for one central target position on each chip.

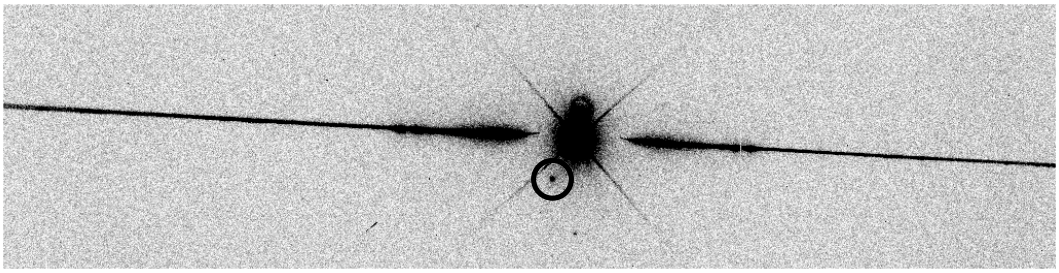

Figure 1: Sum of a direct image (F300X) and a G280 exposure of the continuum point source. A black circle marks the position of the source on the direct image. The prominent 0th order appears at the centre of the image (with spikes); the grism +1st and higher positive orders can be seen extending towards the left and the negative orders to the right. There is extended overlap between all orders. The full extent of the detector (4096 pixels) is shown in the x-direction while the y-axis shows a 1024 sub-array.

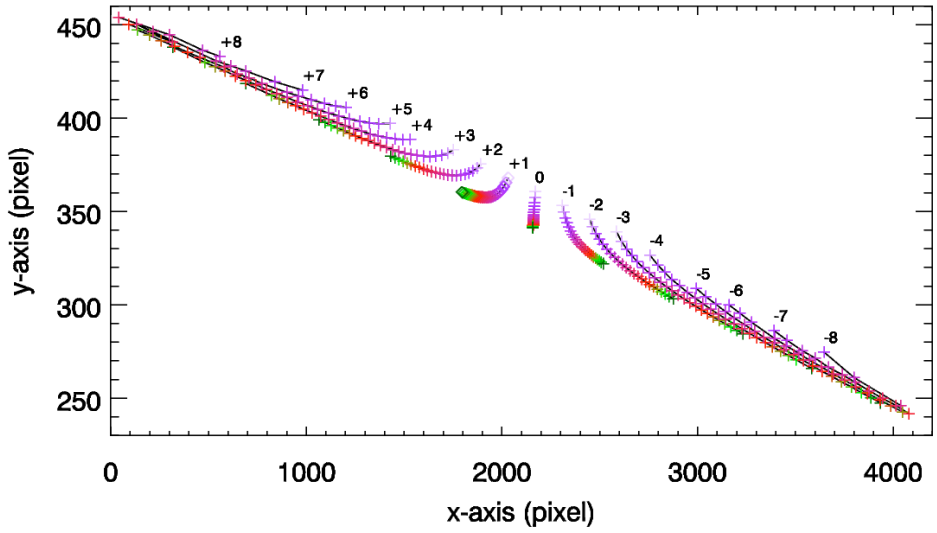

Figure 2: Schematic representation of traces in orders +8 to -8 as derived from monochromator steps obtained during TV2. For each order, colours visualize wavelength from pale purple to green for wavelengths of 200 to 530nm, respectively.

In order to achieve a good trace accuracy (≤1 pixel), a 4th order polynomial fit was needed for all orders apart from the 0th order where a 3rd order polynomial was sufficient. The traces show a strong curvature towards short wavelengths as can be

seen in Figure 3. Although the overall trace shapes are similar for all positive (or negative) orders, they are not identical and individual fits are made for each order. Even for a 4th order polynomial fit, the fit residuals show a clear pattern, which could be removed by using a higher order polynomial. However, for numerical stability considerations, we decided to use the 4th order fits. Once in-orbit data is available, this decision should be reviewed.

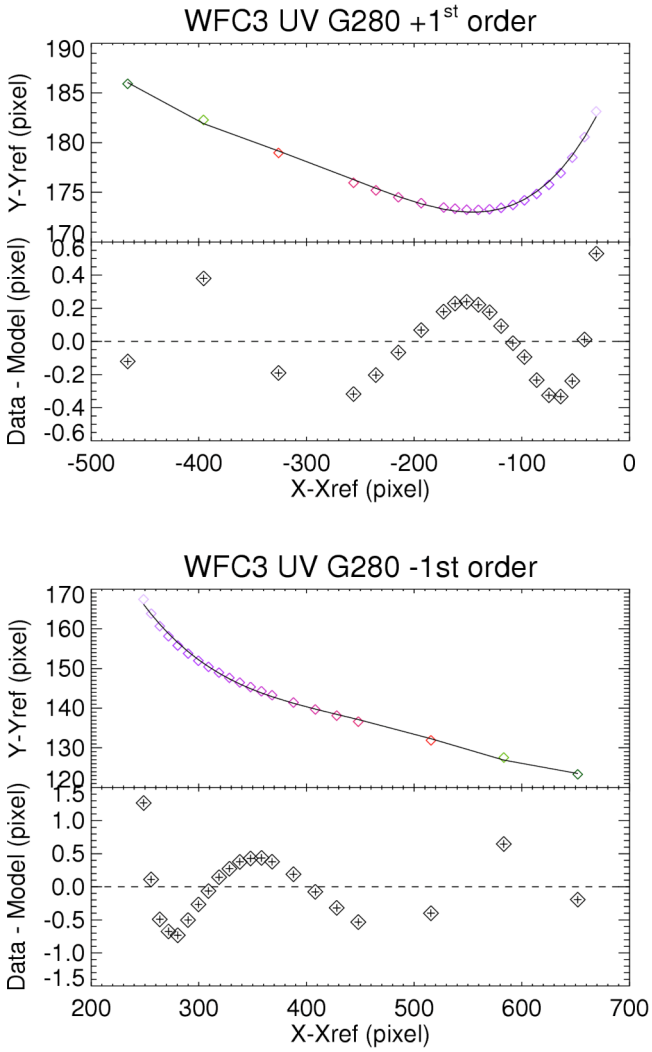

Figure 3: 4th order polynomial fit to the trace of the +1st and -1st orders on Chip 1 as determined in TV3. Monochromator steps between 200 and 815nm are fitted. Colours visualize wavelength from pale purple to green for wavelengths of 200 to 815nm, respectively. See also Figure 2.

Table 4: Trace descriptions for G280 Chip1. Errors are given in brackets.

Term	DYDX_?_0	DYDX_?_1	DYDX_?_2	DYDX_?_3	DYDX_?_4
0th order	4.1398677E+00	1.5685682E+00	-	-	-
BEAM B	(6.0800867E-02)	(6.0605864E-04)	-	-	-
+1st order	1.9035637E+02	3.0160779E-01	1.7547267E-03	3.9119801E-06	3.2031808E-09
BEAM A	(1.6840510E-02)	(4.4718009E-04)	(3.6683026E-06)	(1.1406525E-08)	(1.1778691E-11)
-1st order	4.9140241E+02	-2.7960966E+00	8.5309123E-03	-1.1722711E-05	5.9642521E-09
BEAM C	(5.1146701E-01)	(5.0887490E-03)	(1.8371612E-05)	(2.8531859E-08)	(1.6104306E-11)
+2nd order	2.1742115E+02	2.5505254E-01	6.6723924E-04	6.3943018E-07	2.2556091E-10
BEAM D	(5.3445557E-02)	(4.8127141E-04)	(1.4615993E-06)	(1.7937981E-09)	(7.6154505E-13)
-2nd order	3.5885933E+02	-9.6754140E-01	1.5846974E-03	-1.2161933E-06	3.4478205E-10
BEAM E	(2.7730226E-01)	(1.6161080E-03)	(3.3775688E-06)	(3.0034139E-09)	(9.6136012E-13)
+3rd order	2.3480514E+02	2.1042072E-01	3.6999542E-04	2.2749238E-07	5.1358219E-11
BEAM F	(7.3647799E-02)	(3.9963618E-04)	(7.4321442E-07)	(5.6570448E-10)	(1.5032485E-13)
-3rd order	3.1181273E+02	-5.3013005E-01	5.6668802E-04	-3.0027033E-07	5.8952102E-11
BEAM G	(2.2149148E-01)	(9.1617890E-04)	(1.3518675E-06)	(8.4469119E-10)	(1.8922306E-13)

Table 5: Trace descriptions for G280 Chip2. Errors are given in brackets

	DYDX_?_0	DYDX_?_1	DYDX_?_2	DYDX_?_3	DYDX_?_4
0th order	-1.0147548E+01	1.7016828E+00	-	-	-
BEAM B	(6.0692216E-02)	(6.1800696E-04)	-	-	-
+1st order	1.8568143E+02	3.3151856E-01	1.8772321E-03	4.2478226E-06	3.5294661E-09
BEAM A	(1.6946190E-02)	(4.5841990E-04)	(3.8319296E-06)	(1.2145179E-08)	(1.2785959E-11)
-1st order	4.9551373E+02	-2.9218126E+00	9.1269755E-03	-1.2788866E-05	6.6354836E-09
BEAM C	(5.1218336E-01)	(5.2015165E-03)	(1.9168137E-05)	(3.0386435E-08)	(1.7507048E-11)
+2nd order	2.1345223E+02	2.7992711E-01	7.0644129E-04	6.8588733E-07	2.4495866E-10
BEAM D	(5.3667685E-02)	(4.9285625E-04)	(1.5263762E-06)	(1.9104205E-09)	(8.2720147E-13)
-2nd order	3.5662116E+02	-9.8866925E-01	1.6666712E-03	-1.3023964E-06	3.7594456E-10
BEAM E	(2.7918246E-01)	(1.6597213E-03)	(3.5383261E-06)	(3.2095707E-09)	(1.0480294E-12)
+3rd order	2.2033659E+02	1.7867510E-01	2.9813427E-04	1.7771521E-07	3.9105222E-11
BEAM F	(8.9983698E-02)	(4.8030053E-04)	(8.8616782E-07)	(6.7347031E-10)	(1.7952304E-13)
-3rd order	3.0941814E+02	-5.3659328E-01	5.9350805E-04	-3.1868106E-07	6.3266187E-11
BEAM G	(2.2054091E-01)	(9.3146985E-04)	(1.4031750E-06)	(8.9495899E-10)	(2.0462173E-13)

4.2. Wavelength solutions

The trace definitions derived in Section 4.1 were inserted into a configuration file for the spectral extraction software (aXe), and each of the monochromator spectra were then extracted using the standard aXe task AXECORE. The software automatically extracts the spectral orders as separate "beams", defined with respect to the location of the object in the direct image. The extracted spectra produced by aXe were then analyzed using custom-built IDL scripts where the (X-X_{ref}) location of the peak of each monochromator spot was measured by fitting a Gaussian.

For the determination of the dispersion solution only wavelengths between 200 and 515 nm were used since this allowed good fits and the sensitivity drops markedly at longer wavelength (see also Figures 5 & 6). Furthermore, for wavelengths larger than about 390nm there is overlap with the $+2^{nd}$ order trace, thus reducing the usefulness of the red wavelength range. The restricted wavelength solutions were found to be well approximated by a 3^{rd} order polynomial (see Figure 4). Only the 0^{th} order shows a highly non-linear solution, which is nevertheless approximated by a 3^{rd} order polynomial since it is not used for science. The final, adopted wavelength solutions are shown in Tables 6 and 7.

For G280 the standard deviation around the fit was typically 2.5 Å for the $+1^{st}$ order (mean linear dispersion ~14 Å/pixel) and 3-8 Å for the other orders. Within the uncertainties, the wavelength solutions behave as expected, with the $+1^{st}$ and -1^{st} orders having similar dispersions, and the 2^{nd} and 3^{rd} orders having dispersions of 1/2 and 1/3 of that of the 1^{st} order, respectively. The 0^{th} order spectra also show a small dispersion with a linear term of about 130 Å/pixel.

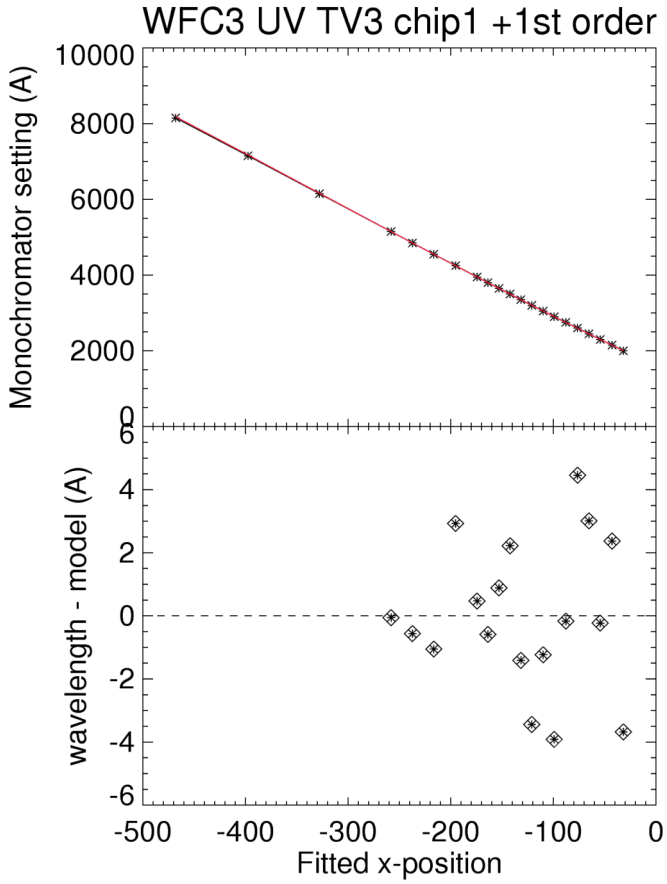

Figure 4: Dispersion solution for G280 +1st order on Chip 1. The fitting range includes only monochromator settings between 200 and 515nm; the three datapoints at large negative values of X (wavelengths 615, 715, and 815nm) are shown in the top plot, but not fitted and thus outside the plotting range of the bottom panel.

Table 6: Dispersion description for G280 Chip 1. Errors are given in brackets.

Term	DLDP_?_0	DLDP_?_1	DLDP_?_2	DLDP_?_3
0th order	4.52098E+06	-6.92001E+04	3.53413E+02	-6.01910E-01
BEAM B	(4.91594E+05)	(7.72944E+03)	(4.04825E+01)	(7.06254E-02)
+1st order	1.59531E+03	-1.26925E+01	5.71377E-03	5.86511E-06
BEAM A	(5.03689E+00)	(1.37587E-01)	(1.07498E-03)	(2.47892E-06)
-1st order	-1.49848E+04	7.40759E+01	-1.07642E-01	6.50678E-05
BEAM C	(1.58289E+03)	(9.23233E+00)	(1.78144E-02)	(1.13717E-05)
+2nd order	7.54974E+02	-7.36277E+00	-9.28759E-04	-9.40626E-07
BEAM D	(2.09847E+01)	(1.83875E-01)	(4.99752E-04)	(4.24898E-07)
-2nd order	-3.05564E+03	1.55764E+01	-1.18203E-02	5.66257E-06
BEAM E	(2.35275E+02)	(1.14090E+00)	(1.80585E-03)	(9.33446E-07)
+3rd order	3.09481E+02	-5.81707E+00	-1.67089E-03	-8.27550E-07
BEAM F	(6.02522E+01)	(3.14897E-01)	(5.17451E-04)	(2.68868E-07)
-3rd order	-1.81391E+03	8.75169E+00	-4.15036E-03	1.49429E-06
BEAM G	(1.35862E+02)	(5.00812E-01)	(5.98879E-04)	(2.32548E-07)

Table 7: Dispersion description for G280 Chip 2. Errors are given in brackets.

Term	DLDP_?_0	DLDP_?_1	DLDP_?_2	DLDP_?_3
0th order	4.48446E+06	-6.60149E+04	3.24245E+02	-5.31101E-01
BEAM B	(4.92716E+05)	(7.44987E+03)	(3.75211E+01)	(6.29467E-02)
+1st order	1.59431E+03	-1.28866E+01	6.20498E-03	6.50182E-06
BEAM A	(5.53615E+00)	(1.53850E-01)	(1.22339E-03)	(2.87226E-06)
-1st order	-1.58762E+04	7.83460E+01	-1.14854E-01	6.94363E-05
BEAM C	(1.75574E+03)	(1.02251E+01)	(1.97068E-02)	(1.25688E-05)
+2nd order	7.26147E+02	-7.71643E+00	-1.50625E-03	-1.45100E-06
BEAM D	(2.73901E+01)	(2.44149E-01)	(6.75288E-04)	(5.84506E-07)
-2nd order	-3.43574E+03	1.75855E+01	-1.48514E-02	7.27285E-06
BEAM E	(3.66170E+02)	(1.80500E+00)	(2.90485E-03)	(1.52698E-06)
+3rd order	3.62952E+02	-5.68364E+00	-1.33245E-03	-6.70603E-07
BEAM F	(4.96545E+01)	(2.65521E-01)	(4.46281E-04)	(2.37107E-07)
-3rd order	-1.78315E+03	8.80951E+00	-4.17100E-03	1.52752E-06
BEAM G	(1.39453E+02)	(5.24496E-01)	(6.39938E-04)	(2.53535E-07)

Using the above-described trace and wavelength calibrations with the aXe software to extract a so called "stamp image" for the $+1^{st}$ order, one can examine the contamination (overlap) from the $+2^{nd}$ order spectral trace. In Figure 5 we show a wavelength calibrated and rectified stamp image extracted from a combination of monochromomator steps. The overlap of $+1^{st}$ and $+2^{nd}$ orders in the x-direction for wavelengths larger than about 390 nm in the $+1^{st}$ order is clearly visible.

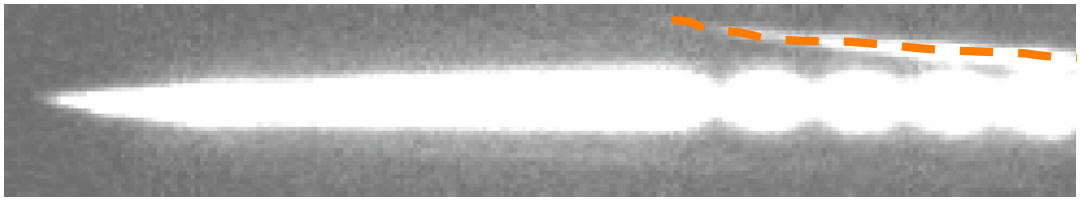

Figure 5: Wavelength calibrated and rectified stamp image of the +1st order spectrum taken from a combination of monochromator steps. Some of the distinct monochromator steps can be seen to the right while others are blended. The wavelength range extends from about 180 to 525nm with wavelength increasing from left to right. Note, the wavelength direction is reversed on the original CCD images; see Figure 1 and 2. The y-axis shows a 44 pixel wide range. The spectral traces of the +1st and +2nd (marked in orange) orders overlap in the x-direction for wavelengths greater than about 390 nm in the +1st order.

4.3. Absolute throughput calibrations

For each of the calibrated monochromator settings (see also Section 3) and all visible orders, the detected counts were measured with the IRAF task imexam. The aperture radius was set to 40 pixels. The ratio of detected flux (using a gain of 1.56 e/DN and 1.57 e/DN for Chips 1 and 2, respectively; see also Baggett 2008) versus the incoming flux as recorded in the image headers (keyword OSFLUX, given as flux per second) gives then the instrument efficiency. Figures 6 and 7 present the efficiency curves for WFC3/UVIS G280 for CCD Chip 1 and Chip 2, respectively. The plots show the efficiency of WFC3/UVIS G280 as measured in TV3 but do not include any contributions from the Optical Telescope Assembly (OTA) throughput. The position of the light source in a direct image corresponds approximately to x=1149, y=896 on Chip 1 and x=1142, y=1171 on Chip 2. The former coordinates were estimated from the position of the 0th order in the dispersed images due to a lack of direct images.

The peak efficiency of ~23% and ~29% is reached at 240nm in the +1st order for Chip 1 and Chip 2, respectively. There is good agreement between the measurements in TV2 and TV3 for the first order throughput on Chip 1. The efficiency is a strong function of wavelength starting with ~6% at the bluest wavelength probed by the TV3 calibrations (190nm) and steeply declining again after the peak efficiency. Most notable, the 0th order carries more power than the 1st order for wavelength above ~320nm. The peak efficiency of ~28% in the 0th order is reached at 600-700nm with significant throughput measured out to 1000nm. Furthermore, the –1st order carries significant power with an efficiency of 4-5% from 230 - 340nm.

Tables 7 and 8 present the efficiency measurements in tabular form for the WFC3/UVIS G280 grism on Chips 1 and 2, respectively. We note that, due to the large throughput for the 0th order at wavelengths greater than 400nm and large wavelength intervals per pixel covered for this order, saturation effects are to be expected. For the white light continuum lamp exposures obtained during the ground calibration campaign, the ratio of the brightest pixel in the 0th order to the brightest pixel in the +1st order is about 200.

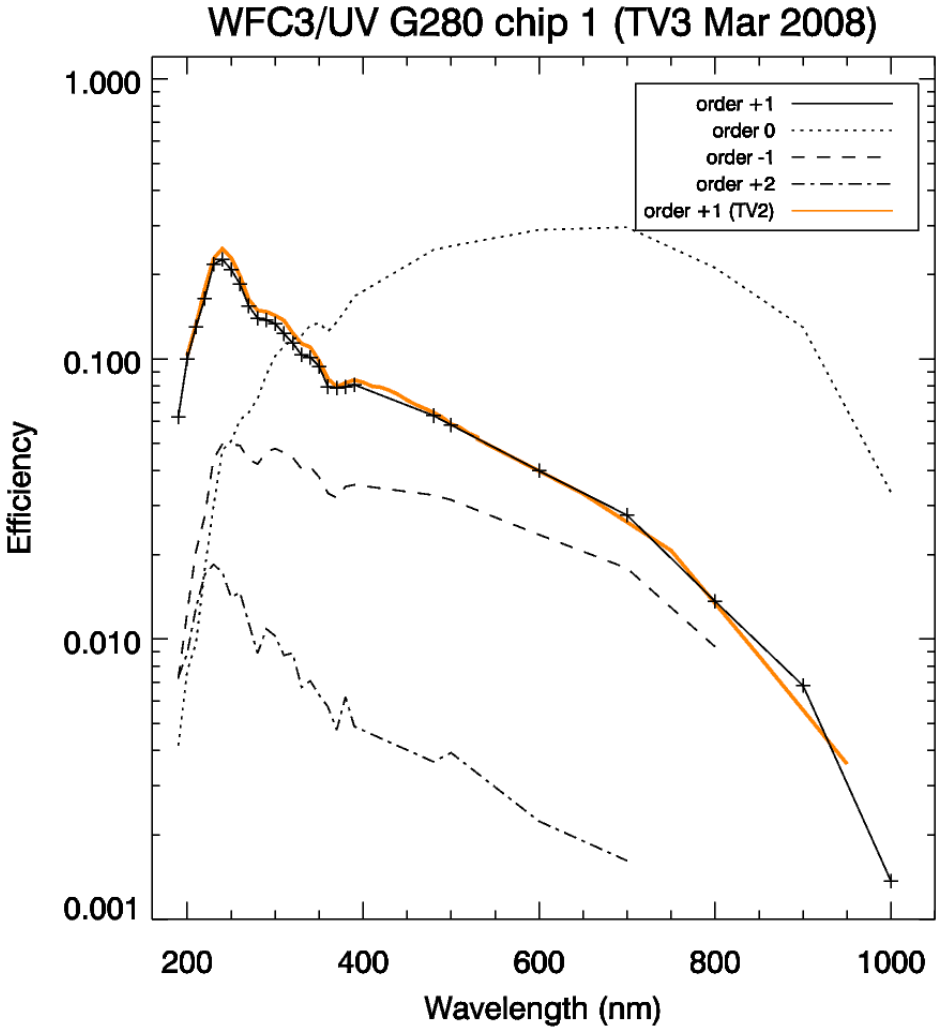

Figure 6: Instrument efficiency of the first few orders for the WFC3/UVIS G280 grism on Chip 1 as a function of wavelength. For comparison the solid orange line shows the measurements for the 1st order on Chip 1 from TV2.

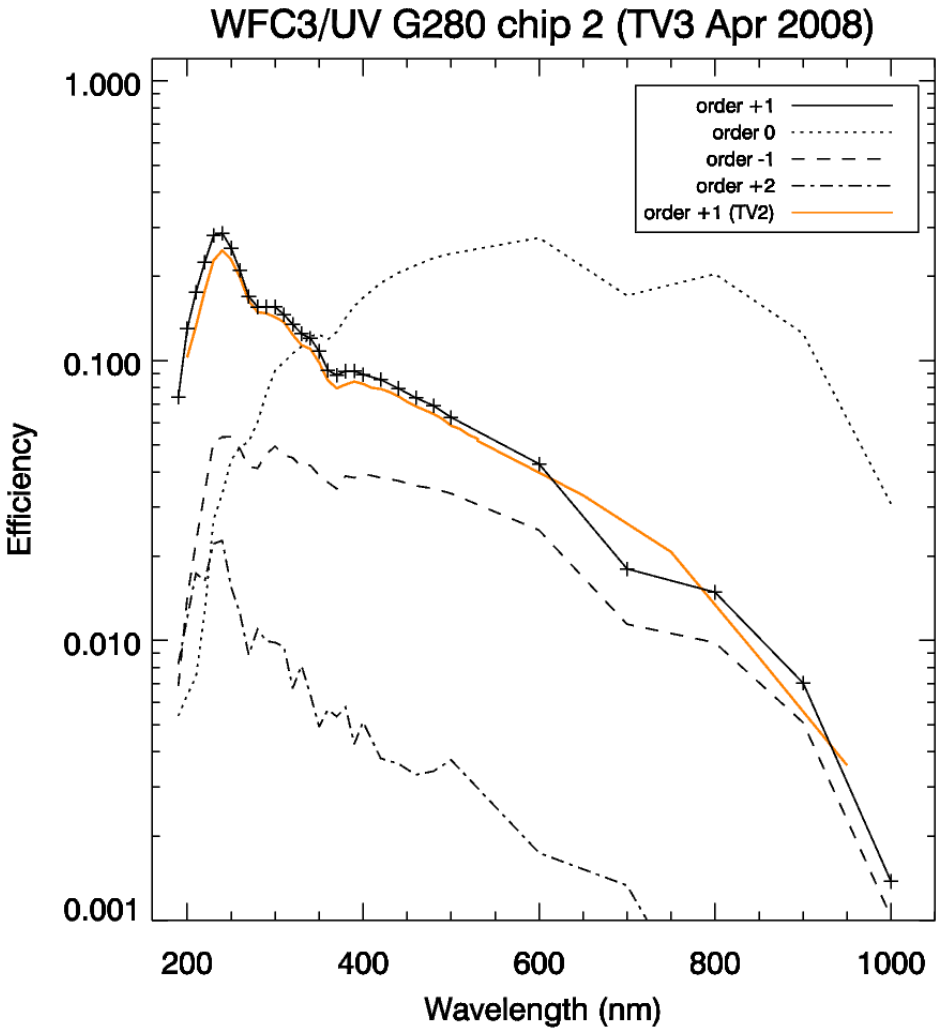

Figure 7: Instrument efficiency of the first few orders for the WFC3/UVIS G280 grism on Chip 2 as a function of wavelength. For comparison the solid orange line shows the measurements for the 1st order on Chip 1 from TV2.

Table 8: Instrument efficiency for WFC3/UVIS G280 Chip 1

Wavelength (nm)	0th	+1st	+2nd	-1st	-2nd	+3rd	-3rd
190	0.0042	0.0621	0.0073	0.0072	0.0014	0.0019	-
200	0.0077	0.0998	0.0089	0.0124	0.0009	0.0014	-
210	0.0097	0.1303	0.0129	0.0206	0.0039	0.0040	0.0025
220	0.0178	0.1645	0.0170	0.0275	0.0060	0.0064	0.0050
230	0.0299	0.2179	0.0185	0.0441	0.0057	0.0055	0.0042
240	0.0473	0.2271	0.0173	0.0497	0.0050	0.0047	0.0038
250	0.0509	0.2087	0.0141	0.0495	0.0039	0.0032	0.0023
260	0.0606	0.1853	0.0147	0.0492	0.0061	0.0055	0.0047
270	0.0643	0.1548	0.0114	0.0437	0.0052	0.0045	0.0039
280	0.0722	0.1398	0.0089	0.0422	0.0032	0.0028	-
290	0.0881	0.1377	0.0109	0.0466	0.0053	0.0049	-
300	0.1025	0.1338	0.0103	0.0479	0.0054	0.0047	-
310	0.1110	0.1232	0.0087	0.0463	0.0040	0.0037	-
320	0.1175	0.1140	0.0089	0.0445	0.0046	0.0043	-
330	0.1212	0.1034	0.0067	0.0405	0.0050	0.0048	-
340	0.1319	0.1014	0.0071	0.0412	0.0038	0.0035	-
350	0.1345	0.0941	0.0063	0.0379	0.0037	0.0032	-
360	0.1254	0.0796	0.0057	0.0332	0.0037	0.0035	-
370	0.1356	0.0788	0.0047	0.0319	0.0027	0.0031	-
380	0.1497	0.0794	0.0062	0.0350	0.0045	0.0041	-
390	0.1676	0.0809	0.0049	0.0356	0.0030	0.0025	-
480	0.2455	0.0628	0.0036	0.0327	-	-	-
500	0.2532	0.0581	0.0039	0.0314	-	-	-
600	0.2895	0.0399	0.0022	0.0236	-	-	-
700	0.2956	0.0277	0.0016	0.0179	-	-	-
800	0.2119	0.0136	-	-	-	-	-
900	0.1298	0.0068	-	-	-	-	-
1000	0.0334	0.0014	-	-	-	-	-

Table 9: Instrument efficiency for WFC3/UVIS G280 Chip 2

Wavelength (nm)	0^{th}	$+1^{st}$	$+2^{nd}$	-1^{st}	-2^{nd}	$+3^{rd}$	-3^{rd}
190	0.0054	0.0741	0.0082	0.0069	0.0009	0.0023	0.0004
200	0.0064	0.1300	0.0120	0.0142	0.0017	0.0033	0.0002
210	0.0074	0.1755	0.0174	0.0225	0.0057	0.0039	0.0039
220	0.0127	0.2252	0.0163	0.0341	0.0079	0.0052	0.0014
230	0.0270	0.2801	0.0222	0.0514	0.0088	0.0102	0.0059
240	0.0335	0.2855	0.0228	0.0533	0.0101	0.0050	0.0018
250	0.0441	0.2526	0.0155	0.0534	0.0061	0.0063	0.0030
260	0.0491	0.2104	0.0125	0.0484	0.0052	0.0057	0.0030
270	0.0513	0.1697	0.0089	0.0418	0.0038	0.0036	0.0057
280	0.0603	0.1556	0.0110	0.0413	0.0066	0.0035	0.0020
290	0.0764	0.1557	0.0100	0.0464	0.0059	0.0058	0.0043
300	0.0923	0.1556	0.0098	0.0494	0.0062	0.0061	0.0047
310	0.0988	0.1460	0.0095	0.0459	0.0061	0.0033	0.0021
320	0.1062	0.1349	0.0068	0.0450	0.0039	0.0040	0.0027
330	0.1124	0.1249	0.0081	0.0418	0.0036	0.0034	0.0044
340	0.1225	0.1204	0.0064	0.0423	0.0043	0.0041	0.0030
350	0.1241	0.1080	0.0049	0.0389	0.0052	0.0031	0.0022
360	0.1192	0.0923	0.0057	0.0367	0.0042	0.0046	0.0033
370	0.1268	0.0887	0.0053	0.0348	0.0039	0.0024	0.0033
380	0.1420	0.0917	0.0058	0.0387	0.0043	0.0024	0.0035
390	0.1567	0.0918	0.0043	0.0382	0.0031	0.0032	0.0023
400	0.1679	0.0892	0.0051	0.0395	0.0039	0.0040	-
420	0.1895	0.0856	0.0038	0.0382	0.0045	0.0026	-
440	0.2061	0.0796	0.0036	0.0372	0.0025	0.0027	-
460	0.2193	0.0736	0.0033	0.0357	0.0037	0.0026	-
480	0.2328	0.0691	0.0034	0.0349	0.0027	0.0028	-
500	0.2414	0.0627	0.0037	0.0335	0.0030	0.0032	-
600	0.2750	0.0427	0.0017	0.0248	-	-	-
700	0.1709	0.0180	0.0013	0.0114	-	-	-
800	0.2042	0.0149	0.0004	0.0098	-	-	-
900	0.1251	0.0070	-	0.0051	-	-	-
1000	0.0308	0.0014	-	0.0010	-	-	-

4.4. Aperture corrections

Aperture corrections were derived for the G280 grism in the $+1^{st}$ order by using the aXe software to extract a rectified 2-dimensional image of combined monochromator images with wavelength between 200 and 515 nm. In order to avoid contamination by the overlapping $+2^{nd}$ order we separately combined the wavelength steps from 200 to 350 nm and from 365 to 515 nm. The resulting

images were then combined to the final image by adding only the contamination-free parts of the images. The final image is wavelength calibrated and image distortions, as recorded in our trace calibrations, are removed. From this image, covering a large range in spatial direction, sub-apertures (here used in the sense of a diameter) are extracted with the help of IDL scripts and compared to the flux determined in the largest aperture. This procedure is carried out as a function of wavelength in six bins. The resulting aperture correction values are given in Table 10 and Figure 8 shows a graphical representation. About 95% of the flux is concentrated in an aperture (=diameter) of about 15 pixels or 0.6 arcsec.

The equivalent analysis for aperture corrections on Chip 2 give similar results with differences < 2%.

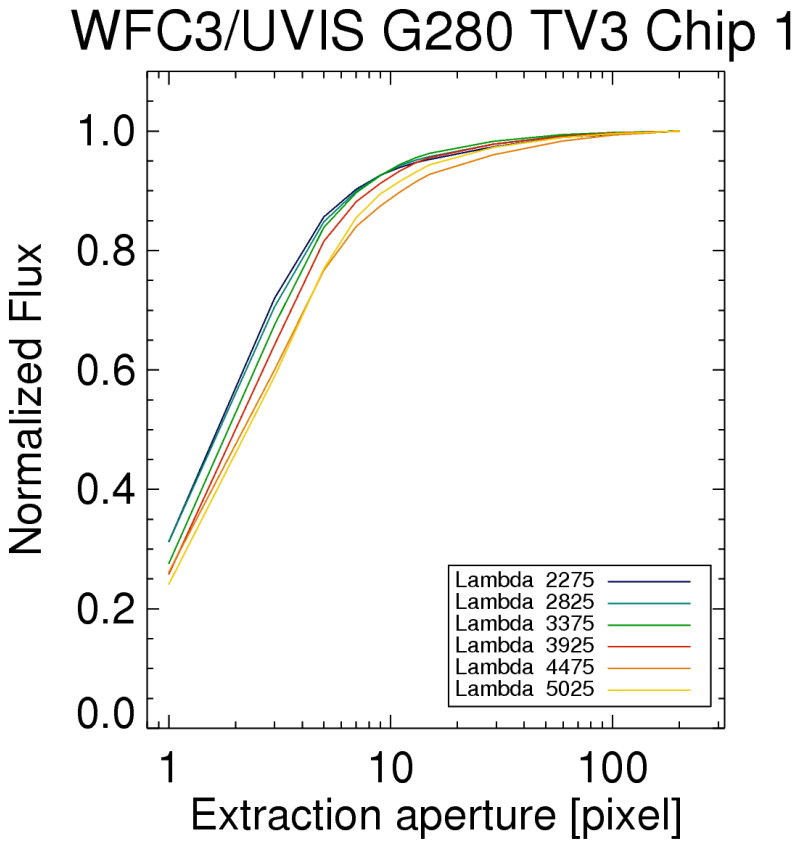

Figure 8: Aperture corrections for G280 as derived in TV3 for Chip 1. The aperture is given as diameter. The wavelengths are quoted in units of Å. The aperture corrections derived for Chip 2 are similar with differences <2%.

Table 10: Aperture corrections for G280 Chip 1 as derived in TV3. The aperture is given as diameter.

Aperture [pixel]	2275 Å	2825 Å	3375 Å	3925 Å	4475 Å	5025 Å
1	0.312	0.312	0.276	0.258	0.261	0.241
3	0.720	0.706	0.676	0.642	0.600	0.589
5	0.856	0.848	0.839	0.815	0.767	0.769
7	0.903	0.899	0.897	0.882	0.840	0.855
9	0.926	0.926	0.926	0.913	0.875	0.895
11	0.939	0.942	0.944	0.933	0.898	0.916
13	0.947	0.951	0.956	0.947	0.915	0.931
15	0.953	0.957	0.963	0.956	0.928	0.944
29	0.974	0.978	0.983	0.978	0.960	0.973
59	0.990	0.992	0.994	0.991	0.983	0.989
101	0.995	0.997	0.998	0.997	0.994	0.996
201	1.000	1.000	1.000	1.000	1.000	1.000

4.5. Flat field determinations

In slitless spectroscopy each pixel can receive any wavelength in the range of the grism, so it is necessary to build a flat-field cube in order to assign a flat-field correction for all pixels and wavelengths. The aXe reduction software employs a flat-field cube in the form of a polynomial fit to the wavelength variation of the flat-field. The input data for constructing a flat-field cube are thus a set of flatfields at specified wavelengths. Using CASTLE and the monochromator, the UVIS channel with the G280 grism was illuminated with light over the wavelength range 2000 to 2400 Å in steps of 200 Å and from 2600 to 5300 Å in steps of 300 Å. The set of measurements at 2000, 2200 and 2400 Å were taken with the monochromator set to produce a 160 Å bandwidth. At these three wavelengths the CASTLE D2 lamp was operated in ambient, and four exposures were combined to produce each flat field image. The exposure times ranged from 4x3600s at 2000 Å to 4x1358s at 2400 Å. The more extensive set of measurements at 2600 Å to 5300 Å were made with the CASTLE Xenon lamp under vacuum conditions and with the monochromator slit producing a bandwidth of 130Å. At each wavelength, two images were obtained with exposure times ranging from 2x3600s (at 2600 Å) to 2x200s (at 5300 Å).

The illumination on each image is fairly uniform but notably on Chip 2 there is a gradient in the illumination to the lower left corner. The illumination pattern was removed by fitting a surface using the IRAF task imsurfit. In order to handle the gradient, separate surface fits were made in two sections, combining the result into a single image before normalization. A spline was used for the fitting function with

order 7 in X and Y. Figure 9 shows one of the monochromatic flats, at 2900A, for Chip 1. The set of 13 normalized flat fields were then fitted pixel-by-pixel by a 3rd order polynomial separately for each chip. The rms on the polynomial fit of the variation of flat field with wavelength had rms values averaged over the whole image, of 0.80% for Chip 1 and 0.74% for Chip 2. Given that the individual images had counts around 10000e per pixel, this is satisfactory but could be slightly improved by a higher order fit (for Chip 1 for example, a 5th order fit brings the image mean of the rms down to 0.64%). Examples of the variation of the flat field with wavelength are shown in Figure 10 for two positions on each chip. The positions were chosen for particularly high and low response values of the normalized flat. The points show the measured flat field averaged over a 3x3 pixel box (where the error bars are the rms on the mean) and the continuous lines display the 3rd order polynomial fit.

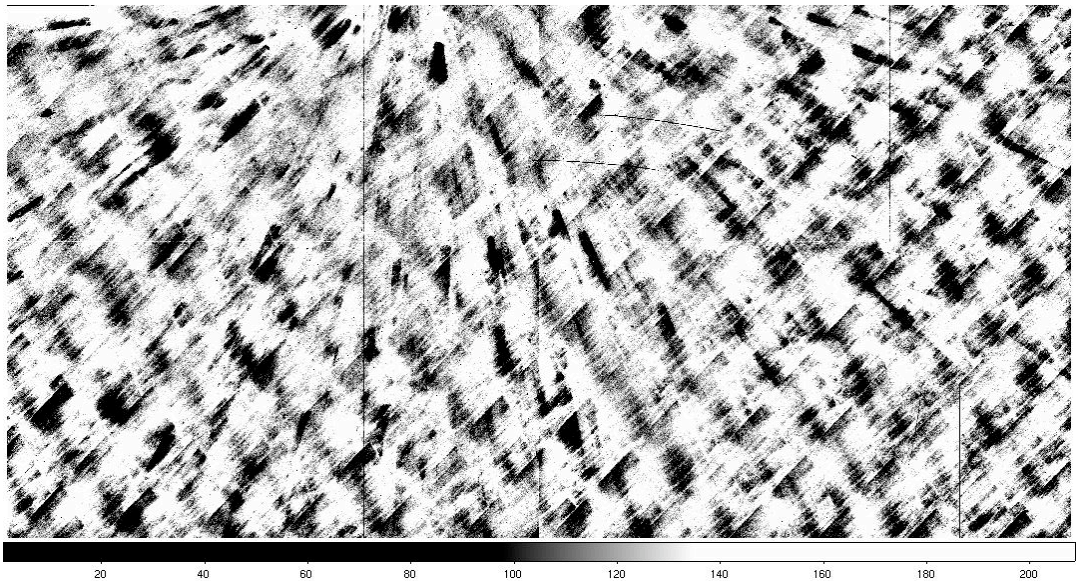

Figure 9: An example of one of the G280 normalized monochromatic flat field maps, at 2900A. The greyscale range is 0.85 to 1.10.

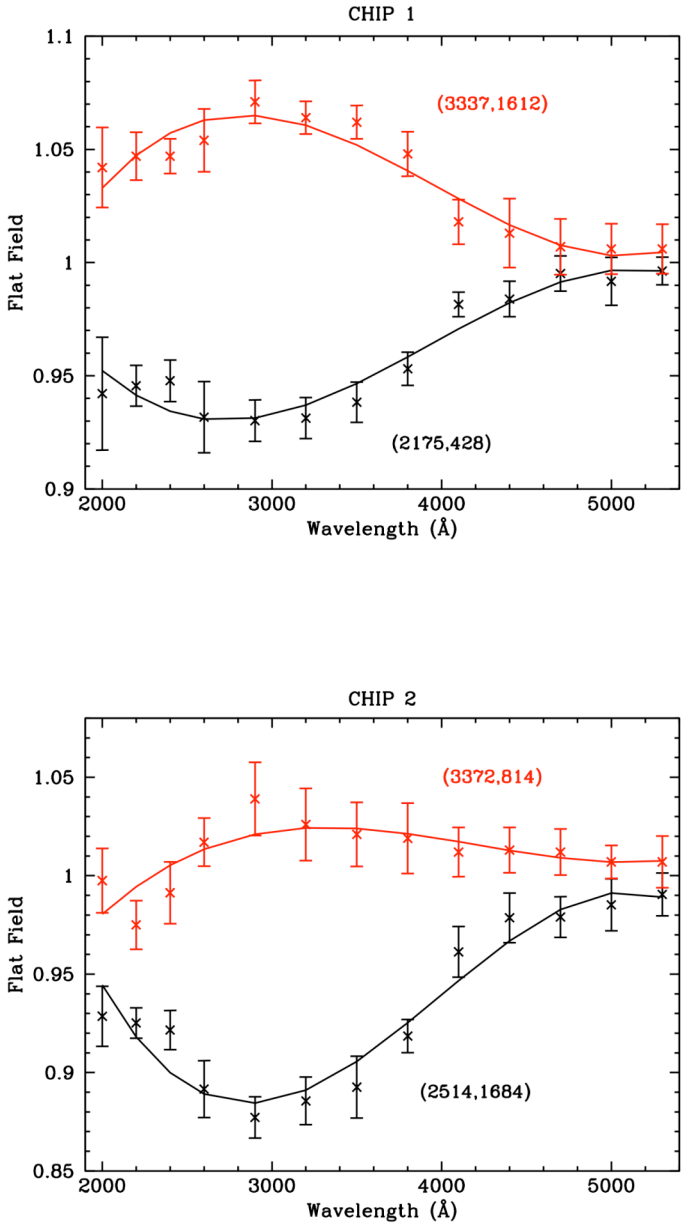

Figure 10: The variation of the flat field for a few selected pixels in each chip is shown. The regions were chosen to illustrate the wavelength dependence of the flat field in low and high response areas. The coordinates of the selected pixels are shown for each set and the points represent the mean over a 3x3 pixel box, with the error bars the rms on the mean. The continuous curve is the 3rd order polynomial fit as stored in the flat field cube.

4.6. Limitations of the ground calibration and application to real observations

In this section we aim to summarize the limits of the WFC3/UVIS G280 calibration derived in this ISR. The calibrations with the flight detectors obtained during TV3 provided trace and wavelength calibrations only for one, central source position for each of the chips (see Table 3). During TV2 calibrations were obtained in a 5-point pattern across the FoV, which demonstrated that the trace and wavelength solutions are a strong function of position within the field of view. These changes (see Figure 11 for an example) are significant and cannot be modelled with linear shifts but rather show a non-linear behaviour. Although the configuration files for the extraction software foresee trace and wavelength calibrations as a function of field-position, the currently available ground calibrations are not sufficient to map these variations. For this reason we can only provide meaningful trace and wavelength solutions in the vicinity of the two standard positions calibrated on the ground during TV3. We estimate that a relative trace and wavelength accuracy of about ½ pixel can be achieved in a radius of about 100 pixels around the standard positions. If the trace and wavelength solutions of the "central" position would be naively applied to the other two positions calibration errors of up to 3.4 pixels and 6.7 pixels for the wavelength and trace, respectively, are to be expected at 2600 Å.

The G280 grism produces spectra in many orders (up to $+12^{th}$ order has been seen) that heavily overlap and cover a (semi-contiguous) region across the whole X-extension of the chips (see also Figure 1). Although spectral overlap between different sources in the FoV is a common feature of slitless spectroscopy, it is a particularly serious problem for the G280 grism. Furthermore, since we currently cannot establish an accurate 2-diminsional trace and wavelength solution, it is impossible to estimate the trace overlap for a given distribution of objects across the FoV. The latter is done for the WFC3/IR grisms and such allows for the estimation of contamination. We conclude that currently the G280 mode is only useful for relatively isolated targets, which are placed at or near to the two calibrated standard positions.

Two further limitations of the G280 grism observations are noteworthy. Firstly, the $+1^{st}$ order spectra overlap in x-direction with the $+2^{nd}$ order spectra for wavelengths larger than about 390nm (see Figure 5). For blue targets this can lead to significant contamination of the $+1^{st}$ order spectra. Secondly, the $+1^{st}$ order efficiency drops markedly beyond 320nm, where in fact the 0^{th} order starts to carry most of the power and reaches a peak efficiency of almost 30% at 600-700nm. Since the 0^{th} order is only mildly dispersed, the rather high efficiency at red optical wavelengths

can lead to severe saturation effects for red sources (see also Figure 1).

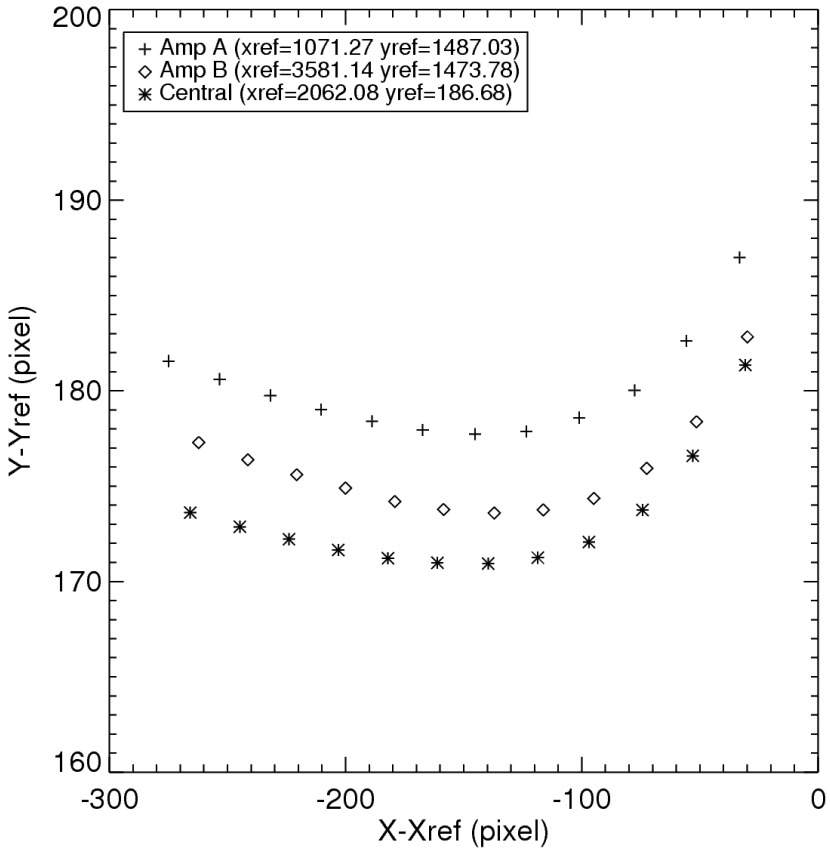

Figure 11: Comparison of +1st order traces relative to the source position determined with monochromator steps in the range 200 to 530nm with a step size of 30nm (the wavelength increases from right to left). The figure shows traces obtained on Chip 2 during TV2 at three different source positions given in the figure inset. Note the differences in y-offset (=Y-Yref) as a function of wavelength and the changes in the wavelength solution as a function of x-pixel position.

5. Conclusions

This ISR presented the WFC3/UVIS G280 grism calibrations carried out during thermal vacuum 2 and 3 (TV2 + TV3). The grism shows highly non-linear dispersion relations and trace definitions for all orders. Typically, 3rd or 4th order polynomials are needed to establish a reasonably accurate (<1 pixel) fit to the calibration data. At least +/-8 orders are visible in deep observations of point-like sources. Additionally, the orders show heavy overlap, especially for higher orders.

The $+1^{st}$ order is contaminated by the $+2^{nd}$ order spectral trace for wavelengths larger than about 390nm. This ISR provides calibrations for $+3^{rd}$ to -3^{rd} orders.

The trace and wavelength solutions show significant variations across the field-of-view (FoV), however, we were not able to characterize them with the sparse sampling of the field obtained during TV2. Henceforth, we report in this ISR trace and wavelength solutions valid only in the vicinity of the central positions on each chip that were calibrated during TV3. These two default positions are reported in Table 3.

The average dispersion in the $+/-1^{st}$ orders is ~14 Å/pixel. The $+1^{st}$ order shows a peak efficiency of 23 and 29% at 240nm, for Chips 1 and 2, respectively. We observe steeply declining efficiencies towards lower and higher wavelengths. The 0^{th} order carries significant power and it becomes the most efficient order for wavelengths greater than about 320nm with a peak efficiency of 29% at 700nm. Due to the small dispersion of the 0^{th} order, saturation is likely to occur, especially for red objects.

Aperture corrections are provided as a function of wavelength. Furthermore, we derive flat-field cubes that provide pixel-to-pixel information as a function of wavelength to an accuracy of about 2%.

The final configuration and sensitivity files can be used in a simulation package (aXeSIM) for HST/WFC3 grism observations, and are available from our Web pages (http://www.stecf.org).

References

Baggett, 2008, WFC3 Instrument Science Report, WFC3-2008-13
Larsen, Bushouse, & Walsh, 2005, ST-ECF Instrument Science Report, WFC3-2005-17
Kümmel, Walsh, Pirzkal, Kuntschner, Pasquali, 2009, PASP in press
Kümmel, Kuntschner, Walsh, 2007, ST-ECF Newsletter, 43, 8